nature climate change

ARTICLES

PUBLISHED ONLINE: 26 OCTOBER 2015 | DOI: 10.1038/NCLIMATE2838

Revaluating ocean warming impacts on global phytoplankton

Michael J. Behrenfeld[1]*, Robert T. O'Malley[1], Emmanuel S. Boss[2], Toby K. Westberry[1], Jason R. Graff[1], Kimberly H. Halsey[3], Allen J. Milligan[1], David A. Siegel[4] and Matthew B. Brown[1]

Global satellite observations document expansions of the low-chlorophyll central ocean gyres and an overall inverse relationship between anomalies in sea surface temperature and phytoplankton chlorophyll concentrations. These findings can provide an invaluable glimpse into potential future ocean changes, but only if the story they tell is accurately interpreted. Chlorophyll is not simply a measure of phytoplankton biomass, but also registers changes in intracellular pigmentation arising from light-driven (photoacclimation) and nutrient-driven physiological responses. Here, we show that the photoacclimation response is an important component of temporal chlorophyll variability across the global ocean. This attribution implies that contemporary relationships between chlorophyll changes and ocean warming are not indicative of proportional changes in productivity, as light-driven decreases in chlorophyll can be associated with constant or even increased photosynthesis. Extension of these results to future change, however, requires further evaluation of how the multifaceted stressors of a warmer, higher-CO_2 world will impact plankton communities.

Ocean warming has been implicated as causing an expansion of the low-chlorophyll, low-productivity central ocean gyres[1–3]. Satellite observations have also shown that broad ocean regions exhibit an inverse relationship between interannual and interdecadal changes in sea surface temperature (SST) and surface phytoplankton chlorophyll concentrations[4–7]. In other words, chlorophyll tends to decrease when temperatures increase, or increase when temperatures decrease. If chlorophyll concentration is simplistically taken as a measure of phytoplankton biomass, then these findings imply a warmer future ocean may be accompanied by decreased phytoplankton stocks and productivity[2,4,8–10]. However, the chlorophyll signal is not so easy to interpret. Chlorophyll concentrations also register physiological adjustments in cellular pigmentation arising from changes in upper ocean light and nutrient conditions[11–14]. These physiological responses can potentially undermine earlier interpretations of the SST–chlorophyll relationship, and thus its extension to future ocean warming impacts[5,7].

Here, we show that physiological changes in cellular pigmentation are often the dominant cause of satellite-observed interannual variations in chlorophyll. This physiological signal includes a clear signature of phytoplankton responses to changing mixed-layer light conditions (that is, 'photoacclimation'). Our findings imply that temperature-correlated decreases in chlorophyll over large ocean areas are often not synonymous with equivalent decreased productivity. To arrive at this conclusion, it was necessary to first revisit mechanisms of light-regulated chlorophyll synthesis to construct a photoacclimation model applicable to the dynamic light environment of the upper ocean. The model was then evaluated against global phytoplankton carbon-to-chlorophyll ratio data (θ, a standard metric of cellular pigmentation), before assessing the contribution of photoacclimation to the satellite chlorophyll record. Our results yield a less dire interpretation of contemporary ocean phytoplankton changes, provide new insight into chlorophyll synthesis regulation, and offer a revised description of photoacclimation that can benefit ocean ecosystem modelling, global productivity estimates, and evaluations of photoprotection in the light-saturated upper ocean.

Mechanisms of photoacclimation

Oxygenic photosynthesis involves coupled electron transport between two pigmented light-harvesting photosystems, termed PSII and PSI (Fig. 1a). An inner-membrane pool of plastoquinone (PQ) molecules functions as the electron shuttle between these photosystems, while simultaneously transporting protons across the photosynthetic membrane (which drives ATP synthesis). When phytoplankton are exposed to a range of increasing light intensities, their photosynthetic rate initially increases with light, but then saturates because ATP and reductant (NADPH) turnover become rate limiting (Fig. 1b). Consequently, electron transport between PSII and PSI progressively 'backs-up' as light increases, causing the PQ pool to become increasingly reduced (that is, in the form of plastoquinole, PQH_2 (Fig. 1b)). The ratio of these oxidized to reduced molecules (that is, the PQ pool 'redox state') thus provides a sensitive measure of the balance between the cell's light-harvesting 'machinery' and its capacity to utilize its photosynthetically generated ATP and NADPH. Phytoplankton use this signal (along with other correlated signals) to regulate chlorophyll synthesis[15–18] (Supplementary Discussion). A predominantly oxidized PQ pool indicates that light harvesting is insufficient, so chlorophyll synthesis is upregulated. Conversely, a pool that is predominantly reduced indicates that chlorophyll concentration is too high, so synthesis is downregulated. This relationship between PQ redox state and chlorophyll synthesis is fundamental to photoacclimation models applied to satellite observations of surface ocean mixed-layer phytoplankton.

[1]Department of Botany and Plant Pathology, Cordley Hall 2082, Oregon State University, Corvallis, Oregon 97331-2902, USA. [2]School of Marine Sciences, 5706 Aubert Hall, University of Maine, Orono, Maine 04469-5741, USA. [3]Department of Microbiology, 220 Nash Hall, Oregon State University, Corvallis, Oregon 97330, USA. [4]Earth Research Institute and Department of Geography, University of California, Santa Barbara, California 93106-3060, USA.
*e-mail: mjb@science.oregonstate.edu

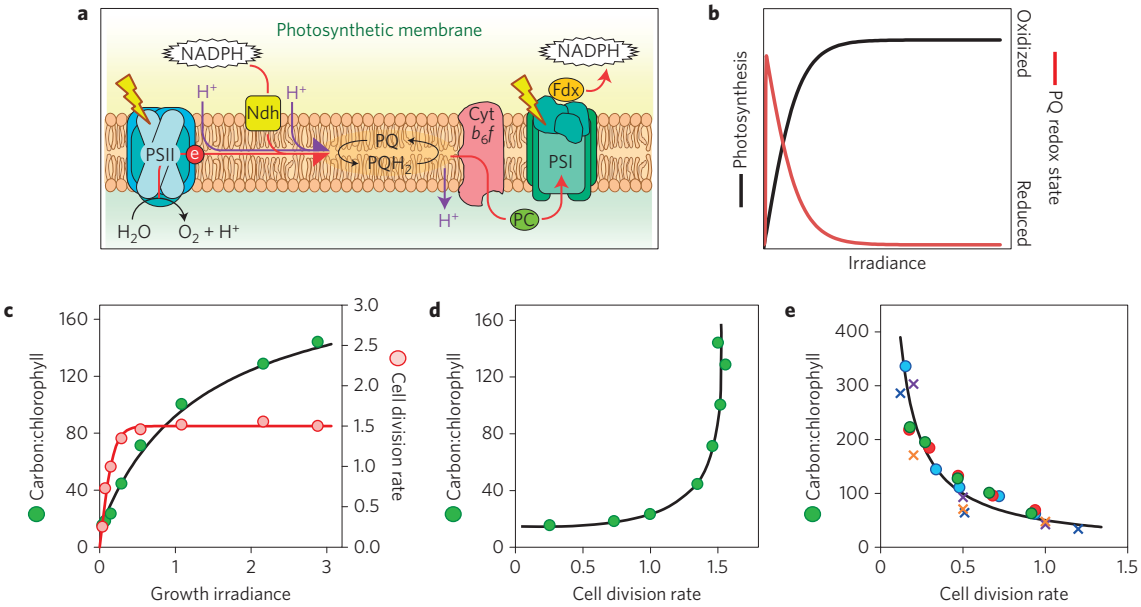

Figure 1 | Photophysiology of phytoplankton. a, Electron transport in photosynthetic membranes between water splitting at PSII and reductant (NADPH) formation after PSI. Also shown is electron transport in darkness from NADPH to the PQ pool through Ndh. PSII, photosystem II. PSI, photosystem I. Cyt b_6f, cytochrome b_6f complex. PQ, plastoquinone. PQH_2, plastoquinole. Fdx, ferredoxin. PC, plastocyanin. NADPH, nicotinamide adenine dinucleotide phosphate. NDH, NADPH dehydrogenase. Yellow 'lightning bolts' signify light absorption by PSII and PSI. **b**, Relationship between photosynthesis and incident irradiance (black line; relative). Photosynthesis initially increases in proportion to irradiance and then becomes light-saturated. The PQ pool is initially reduced in the dark, is oxidized on exposure to light, and then becomes progressively reduced with increasing light (red line; right axis). **c**, Changes in phytoplankton carbon-to-chlorophyll ratio (θ; green symbols; left axis; g C (g Chl)$^{-1}$) and cell division rate (red symbols; right axis; d^{-1}) as a function of growth irradiance (mol photon m^{-2} h^{-1}) as typically observed in nutrient-replete laboratory cultures. Data for *Dunaliella tertiolecta* from ref. 5. **d**, Relationship between θ and cell division rate for nutrient-replete phytoplankton based on data from **c**. **e**, Relationship between θ and cell division rate for steady-state nutrient-limited phytoplankton. Circles: *Thalassiosira weisflogii* under (blue) NO_3, (red) NH_4 and (green) PO_4 limitation. Crosses: NO_3-limited cultures of (blue) *Dunaliella tertiolecta*, (purple) *Thalassiosira weisflogii* and (orange) *Ostreococcus tauri*. Data from refs 11,47.

Whereas reduction of the PQ pool by bright light is widely recognized in photoacclimation models as a regulating factor for chlorophyll synthesis, far less attention has been given to PQ pool redox signalling under conditions of darkness. In the dark, NADPH is mobilized (through stored carbon catabolism) to reduce the PQ pool[19] (Fig. 1a). This process has been documented over extensive open ocean regions through associated changes in phytoplankton fluorescence properties[20–22]. In eukaryotic phytoplankton, this electron transport in the dark is referred to as 'chlororespiration'[23], whereas in prokaryotes it is simply referred to as 'cellular respiration'[24]. A possible implication of this dark PQ redox change is that it may downregulate the chlorophyll synthesis signal. This effect has, to the best of our knowledge, never been considered in models of phytoplankton photoacclimation when deep mixing results in prolonged exposures to darkness.

Photoacclimation in laboratory cultures

Photoacclimation has been thoroughly examined in laboratory phytoplankton cultures[11,12,14,25,26], albeit under light conditions that rarely mimic natural deep-mixing layers. During these experiments, phytoplankton grown over a range of different light levels typically exhibit a strong decrease in θ with decreasing growth irradiance (that is, they become more pigmented; Fig. 1c, green symbols). This response, regulated by PQ redox sensing, is insufficient to prevent reductions in cell division rates at low light (Fig. 1c, red symbols). These parallel responses to changing growth irradiance can be summarized by replotting θ as a function of growth rate (Fig. 1d), thus illustrating how light-driven increases in division rate correspond to strong increases in θ. The opposite relationship is observed in laboratory studies of nutrient stress (Fig. 1e). Here, increases in division rate are associated with strong decreases in θ because faster-growing cells need more chlorophyll (that is, lower θ) to meet demands for photosynthetic ATP and NADPH production.

The dependencies of θ on light and nutrient conditions are critical for understanding why satellites often observe chlorophyll to decrease with increasing temperature and stratification, and what these changes mean in terms of ocean production. More specifically, chlorophyll can decrease because of a decrease in biomass (lower productivity) or an increase in θ. If the change in θ is significant, it can result from an increase in nutrient stress (lower productivity; Fig. 1e) or an increase in growth irradiance (same or increased productivity; Fig. 1d). Interpreting the satellite chlorophyll record therefore requires separating the effects of biomass, nutrients and light, which in turn requires a robust description of photoacclimation for the surface ocean mixed-layer light environment.

Photoacclimation in the ocean's mixed layer

Over the photoperiod, incident sunlight in the mixed layer is attenuated (that is, decreases) exponentially with depth. During midday, photosynthesis near the surface is often light-saturated, meaning that the PQ pool is reduced and the signal for chlorophyll synthesis is 'off' (Fig. 2a). Supersaturating light levels within this 'high light zone' provide no additional redox information, but they do impact calculated values of the average light in the mixed layer. This discrepancy is one reason why average daily irradiance is not an appropriate descriptor of photoacclimation. Recognizing this limitation, an alternative approach has been to describe photoacclimation as a function of the median light level within a well-mixed surface layer (I_{ML}; refs 7,13,27).

$$I_{ML} = \mathrm{PAR}\, e^{-0.5K_d\ \mathrm{MLD}} \quad (1)$$

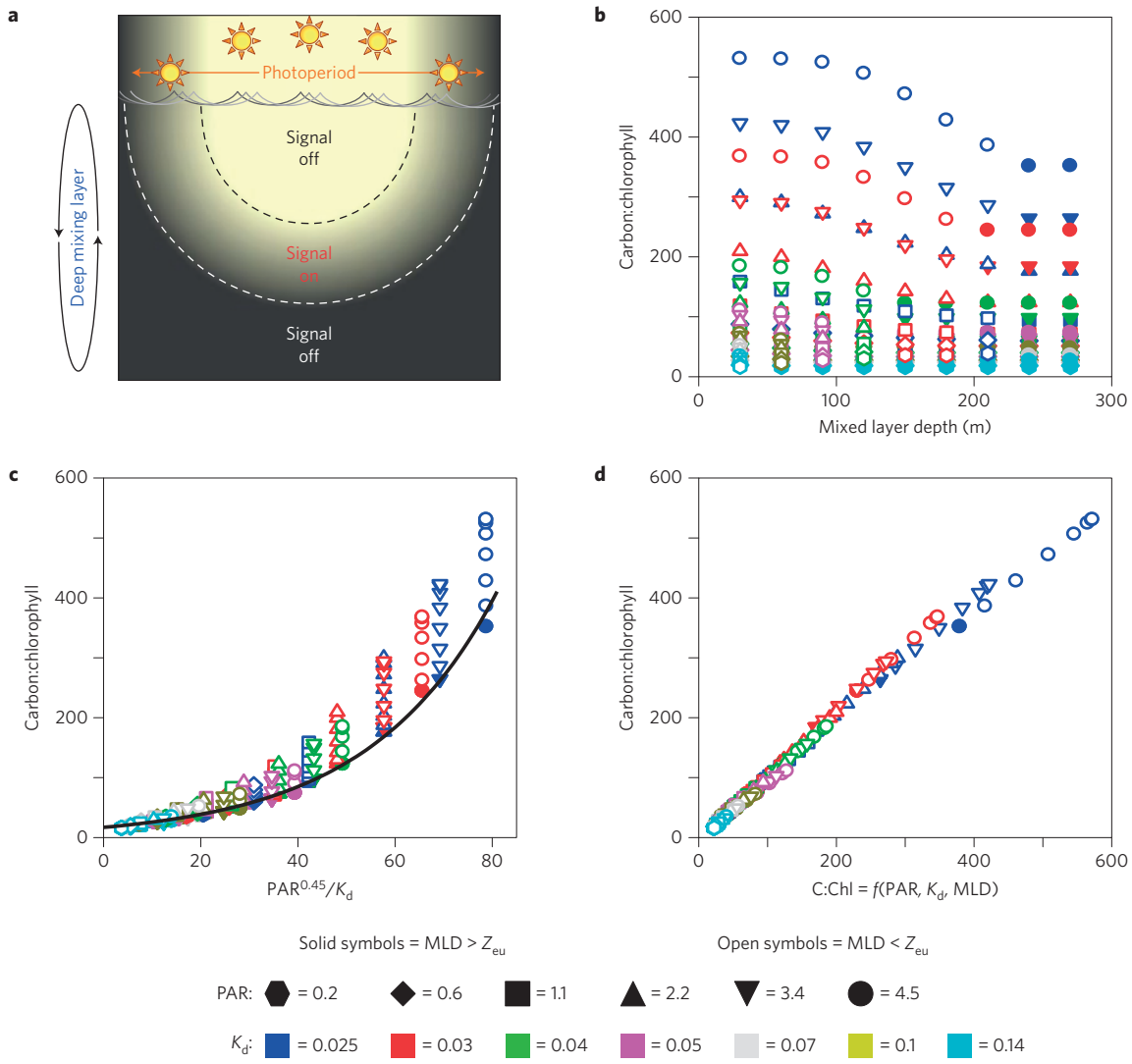

Figure 2 | Modelling photoacclimation in the surface ocean mixed layer. a, Schematic of the mixed-layer (indicated on left) light environment across the photoperiod (top). Redox state of the plastoquinone (PQ) pool is an important regulator of chlorophyll synthesis. Elevated incident sunlight during midday results in light-saturated photosynthesis in the upper photic layer, a reduced PQ pool (Fig. 1), and thus downregulation of chlorophyll synthesis (that is, 'signal off'; area above black dashed line). Similarly, exposure to darkness below the photic depth (white dashed line) results in a biochemical reduction of the PQ pool (Fig. 1) and downregulation of chlorophyll synthesis. In between these two conditions, the PQ pool is oxidized and signals an upregulation of chlorophyll synthesis. Phytoplankton carbon-to-chlorophyll ratios (θ) reflect the balance between these 'on' and 'off' signals, which depends on mixed-layer depth (MLD; m), incident sunlight (PAR; mol of photons $m^{-2}\,h^{-1}$), and the attenuation coefficient for PAR (K_d; m^{-1}). **b**, Steady-state values of θ ($g\,g^{-1}$) from the new photoacclimation model as a function of MLD (m). Solid symbols, deep-mixing scenarios where MLD > photic depth (Z_{eu}; m). Open symbols, shallow-mixing scenarios where MLD < Z_{eu}. **c**, Relationship between model values of θ and $PAR^{0.45}/K_d$ (mol photon $(m\,h)^{-1}$). Black line, equation (2). **d**, Relationship between θ values for the full model (left axis) and from equations (2) and (3) (bottom axis). **b**–**d**, Symbol shapes and colours indicate model combinations of PAR and K_d, as defined in the key at the bottom of the figure.

where PAR is the photosynthetically active radiation (400–700 nm; mol photons $m^{-2}\,h^{-1}$), K_d is the attenuation coefficient (m^{-1}) for downwelling PAR, and MLD is the mixed-layer depth (m). This approach was intended to capture the midpoint light level where the signal for chlorophyll synthesis is 'on' for half of the mixing cycle and 'off' for the other half. However, neither the median nor the average mixed-layer light level account for the chlorophyll synthesis signal being 'off' in the dark (Fig. 2a). Consequently, these descriptors of photoacclimation can overestimate cellular chlorophyll levels when mixing depths exceed the photic zone depth (Z_{eu}; the surface layer of the ocean supporting net photosynthesis).

Recognizing the complexity added by PQ redox signalling in the dark, we first revised the description of mixed-layer photoacclimation before evaluating its significance to global ocean chlorophyll variability. To do this, we initially focused on conditions of deep mixing (that is, MLD > Z_{eu}) and then addressed the effects of mixed-layer shoaling within the photic zone (that is, MLD < Z_{eu}). For deep-mixing scenarios, time- and depth-resolved photosynthesis was calculated for a globally representative range in PAR (0.2–4.5 mol photons $m^{-2}\,h^{-1}$) and K_d (0.02–0.2 m^{-1}). We then determined the changes in the model photosynthesis–irradiance relationship necessary to yield a relationship between θ and net productivity consistent with laboratory findings (Fig. 1d). These deep-mixing solutions were then adjusted for shallow-mixing conditions (MLD < Z_{eu}) based on the relationship between θ and I_{ML} observed in open ocean regions where PAR and K_d are relatively constant (that is, where MLD changes are the primary driver of θ variability)[13,27] (Supplementary Discussion).

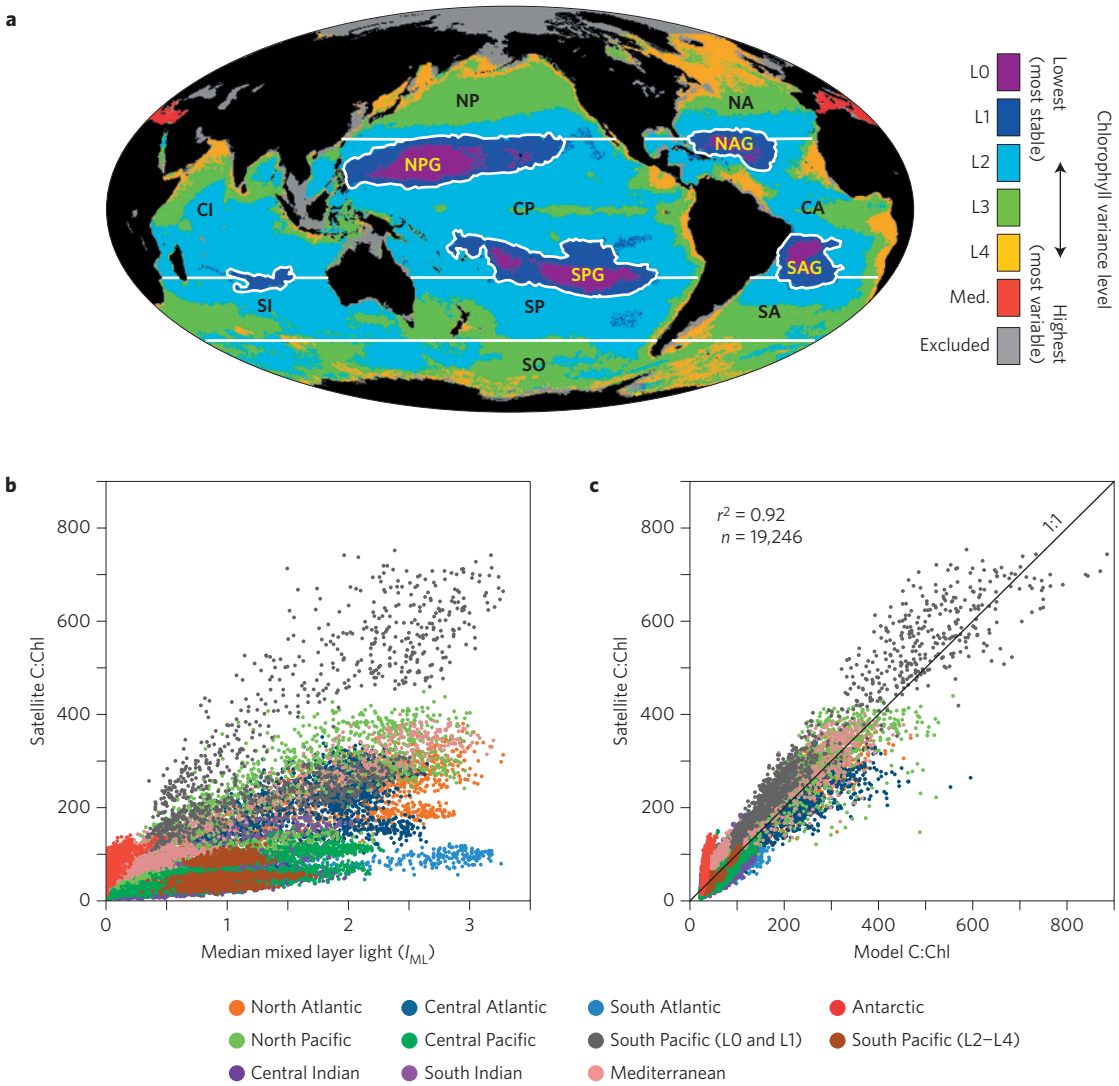

Figure 3 | Carbon-to-chlorophyll (θ) variability in the global ocean. a, The 11-year record of MODIS Aqua 8-day resolution θ data were aggregated into 37 regional bins based on annual variability in chlorophyll, following ref. 13 (right-hand legend; L0, lowest variability (that is, most stable) waters; L4, highest variability waters). Basin designations are: NA, North Atlantic; CA, Central Atlantic; SA, South Atlantic; NP, North Pacific; CP, Central Pacific; SP, South Pacific; CI, Central Indian; SI, South Indian; SO, Southern Ocean; Med., Mediterranean; and Excluded, near-shore and polar waters excluded from the analyses. Central ocean gyres are indicated by the addition of 'G' to two-letter basin designation (for example, SPG, South Pacific Gyre). **b**, Relationship between satellite-observed values of θ (g C (g Chl)$^{-1}$) and median mixed-layer light levels (I_{ML}, mol photons m^{-2} h^{-1}). Colours, ocean basin as defined in the key at the bottom. South Pacific data for the low-variance L0 and L1 bins (black) are separated from higher-variance bins (brown) (see discussion in the main text). **c**, Relationship between satellite-observed θ and model values from equations (2) and (3).

With this limited set of constraints, the model gives a wide range of steady-state solutions for θ (Fig. 2b), which we then analysed with respect to dependencies on PAR, K_d and MLD. For all deep-mixing conditions (solid symbols in Fig. 2c), model values for θ collapsed on a single relationship with $\mathrm{PAR}^{0.45}/K_d$ (Fig. 2c, black line). The dependence here on $\mathrm{PAR}^{0.45}$ results because daily-integrated water-column production initially increases linearly with PAR and then increases more slowly as a greater fraction of the photic zone becomes light-saturated over the photoperiod (that is, water-column productivity is a saturating function of incident PAR; refs 28,29). The dependence of θ on K_d in this relationship results because daily-integrated production for a given MLD and PAR varies inversely with the depth of the photic zone (in Fig. 2a, this region is the area above the dashed white line). The model then adjusts θ upwards from this $\mathrm{PAR}^{0.45}/K_d$ solution when mixing is shallow, because less pigment is needed to sustain a given production rate (open symbols in Fig. 2c).

Results from our full model were used to define a simplified algorithm for application to satellite data. This photoacclimation algorithm is composed of a 'baseline' deep-mixing solution (θ_{DM}; black line in Fig. 2c) and a shallow-mixing correction ($\Delta\theta_{SM}$). Thus, $\theta = \theta_{DM}\Delta\theta_{SM}$, where:

$$\theta_{DM} = c_1\, e^{c_2 \mathrm{PAR}^{0.45}/K_d} \quad (2)$$

with $c_1 = 19$ g C (g Chl)$^{-1}$ and $c_2 = 0.038$ m^{-1}. $\Delta\theta_{SM}$ has a value of 1 for MLD $\geq$ 6 optical depths, whereas for shallower mixing it is calculated as:

$$\Delta\theta_{SM} = \frac{1 + e^{-0.15\mathrm{PAR}}}{1 + e^{-3I_{ML}}} \quad (3)$$

where the parameters in the exponents have units of m^2 h (mol photon)$^{-1}$. The simplified algorithm (equations (2) and (3)) very effectively reproduces θ values from the full model for all

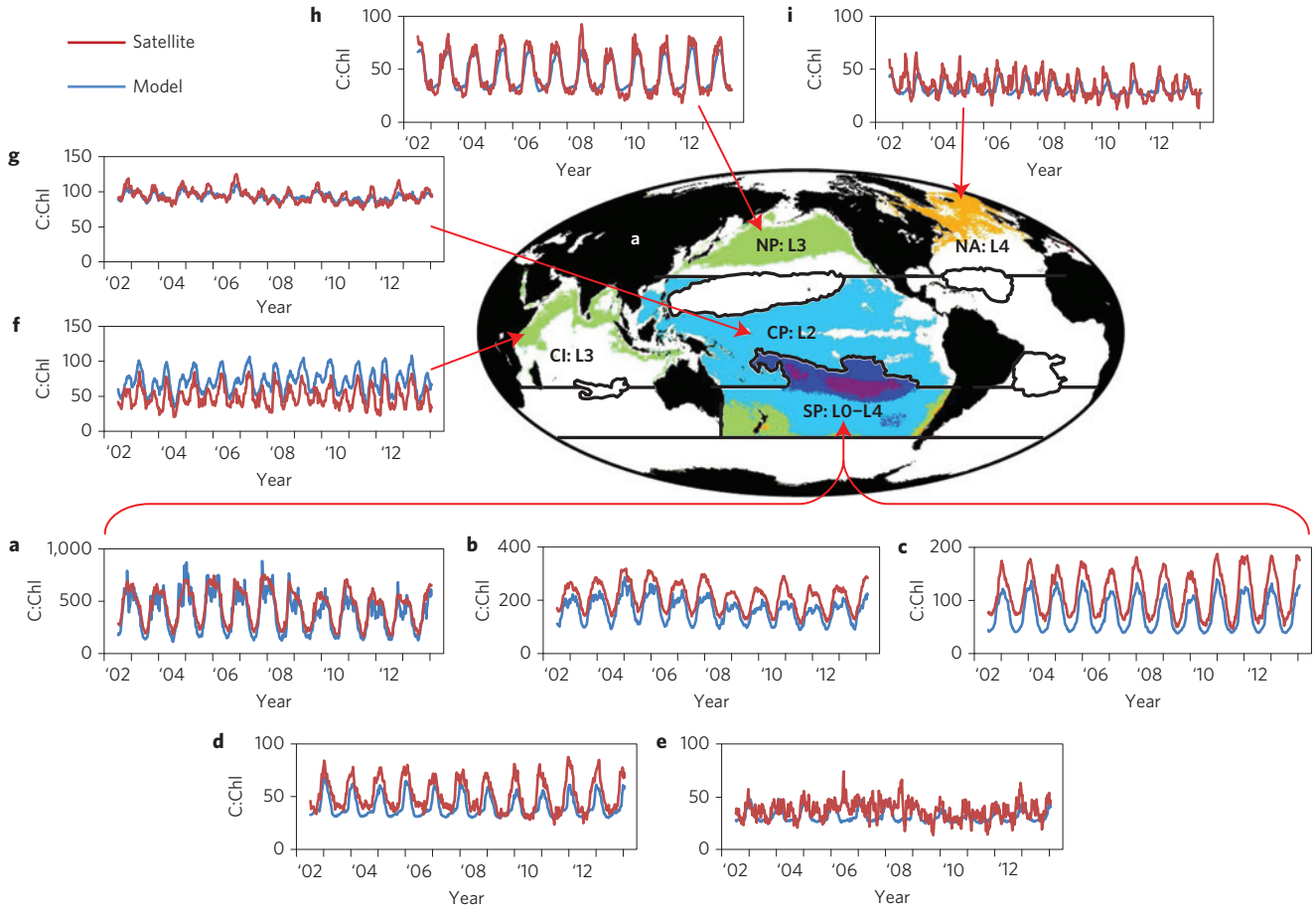

Figure 4 | Temporal patterns in satellite-observed carbon-to-chlorophyll (θ) and model-based variability attributable to photoacclimation. **a**–**e**, Eleven-year records of θ (g C (g Chl)$^{-1}$) for the five South Pacific (SP) variance bins L0 (**a**), L1 (**b**), L2 (**c**), L3 (**d**) and L4 (**e**); note changing *y*-axes scales. **f**, L3 variance bin for the Central Indian (CI) region. **g**, L2 variance bin for the Central Pacific (CP) region. **h**, L3 variance bin for the North Pacific (NP) region. **i**, L4 variance bin for the North Atlantic (NA) region. Red lines, satellite θ record. Blue lines, model estimates (equations (2) and (3)) of θ variability due to photoacclimation.

combinations of PAR, K_d and MLD (Fig. 2d; $r^2 = 0.99$). The photoacclimation algorithm was then applied to an 11-year record of satellite ocean measurements from the MODerate resolution Imaging Spectroradiometer on Aqua (MODIS Aqua, July 2002 to January 2014) (Supplementary Discussion).

Global photoacclimation signature

Satellite measurements provide information on ocean ecosystem properties representative of the actively mixing surface layer, which can vary from tens to hundreds of metres. Retrieved chlorophyll concentrations reflect both phytoplankton abundance and cellular pigmentation (θ). An ability to partition chlorophyll into these two components has arisen from the development of spectral ocean colour inversion algorithms[30–32] and subsequent assessments of phytoplankton carbon (C_{phyto}) from retrieved particulate backscattering coefficients (b_{bp}; refs 13,27). Initially, C_{phyto} products were evaluated against indirect biomass proxies[13,27,33,34], but recent analytical field measurements of C_{phyto} (ref. 35) have now directly validated the satellite algorithm[36]. Simultaneous retrieval of C_{phyto} and Chl allows global evaluations of phytoplankton θ variability.

MODIS Aqua 8-day resolution θ data were aggregated into 37 regional bins[13] (Fig. 3a) and initially compared with median mixed-layer light values (I_{ML}; Fig. 3b). The resultant relationship shows strong regional dependencies that illustrate how fundamental aspects of photoacclimation are insufficiently accounted for by I_{ML} alone. In contrast, the photoacclimation model developed here (equations (2) and (3)) gives predicted values of θ that are far more consistent ($r^2 = 0.92$) with satellite observations for nearly all of the regional bins (Fig. 3c). High-latitude Southern Ocean data are clear outliers in this relationship (Fig. 3c; red symbols), probably reflecting biases in satellite ocean retrievals for this region that are well documented[37,38]. The model also consistently underestimates observed θ values by ~20% for the lowest-variance regions of the South Pacific Gyre (SPG in Fig. 3a; black symbols in Fig. 3c), probably reflecting a particularly high Raman scattering contamination in b_{bp} retrievals for this region of the clearest natural waters on Earth[39].

The model-satellite data comparison shown in Fig. 3c indicates that, at the global scale, photoacclimation is a dominant factor driving θ variability of the mixed layer. The importance of this physiological response is also clear over the smaller dynamic range of θ variability within each regional bin. For example, the five South Pacific bins exhibit single-mode annual cycles in θ with peak values consistently occurring in summer, but with amplitudes that diminish from regions of low to high productivity (red lines in Fig. 4a–e, respectively; note, *y*-axis scale changes between panels). Both the timing and amplitude of these cycles are reliably reproduced by the photoacclimation model (4a–e, blue lines). In productive regions of the Central Indian Ocean, biannual monsoon seasons give rise to a multi-phase annual cycle in θ that contrasts with the South Pacific cycle but again has a strong

photoacclimation signature (Fig. 4f). A multi-phase annual cycle in θ is also observed over broad expanses of the temporally stable Central Pacific, but in this case the cycle has very low amplitude and is driven by Northern- and Southern-Hemisphere seasonal cycles in PAR and MLD encompassed by this expansive trans-equatorial bin (Fig. 4g). In the high-latitude North Pacific, θ exhibits a single-mode annual cycle (Fig. 4h), whereas at similar latitudes in the North Atlantic, θ values are comparatively low and have a less pronounced seasonal cycle reflecting offsetting responses to changing PAR, MLD and K_d (Fig. 4i). For all 37 regional bins, we find that photoacclimation is a primary contributor to observed temporal patterns in θ (Supplementary Fig. 8).

Photoacclimation in a changing climate

Satellite observations of global ocean phytoplankton began in 1978. From these initial measurements to the present, interannual trends in chlorophyll concentration have been observed that are related to climate forcings associated with basin-scale phenomena such as the El Niño–La Niña cycle, Pacific Decadal Oscillation, and Atlantic Meridional Oscillation[4–6,40]. These interannual chlorophyll anomalies are small compared to the biomass-driven seasonal chlorophyll changes in bloom-forming ocean regions, for example, but they are particularly relevant to forecasts of future ocean warming impacts. In general, anomalies in chlorophyll and SST are inversely related, and this finding is often interpreted as implying that phytoplankton biomass and productivity decrease with ocean warming[2,4,8–10].

With an ability to separate chlorophyll changes into biomass and physiological components, it is now possible to evaluate the underlying drivers of interannual anomalies in chlorophyll. Although uncertainties remain in satellite chlorophyll and biomass estimates, what we find is that the interannual anomalies in chlorophyll for the MODIS record are predominantly (>55%) attributed to physiologically driven anomalies in θ, rather than changes in biomass, for over 75% of the global ocean area (Fig. 5a). For ~40% of the global area, changes in θ account for >85% of the chlorophyll anomalies (Fig. 5a). This strong contribution from physiological variability in θ encompasses a diversity of factors, including responses to mixed-layer light and nutrient conditions and shifts in phytoplankton community composition. However, the light-driven component of this variability can now be separated from other factors by applying our photoacclimation model. What we find is that the photoacclimation response accounts for between 10 and >80% of the observed global anomalies in θ for the MODIS record across 40% of the lower-latitude permanently stratified oceans and higher-latitude seasonal seas (Fig. 5b). What this means is that temporal anomalies in chlorophyll do not imply equivalent changes in mixed-layer production. This is because photoacclimation-driven changes in chlorophyll have the opposite relationship to production as nutrient-driven (or biomass-driven) changes in chlorophyll (Fig. 1d,e).

Outlook

Global satellite observations provide a remarkably powerful tool for understanding how ocean ecosystems function today and, ideally, for gaining insights on how these communities may change in the future. Our understanding of ocean ecology, however, inevitably changes (and will continue to change) as improvements are made in ocean colour analysis (for example, inversion algorithms) and descriptions of biological processes (for example, photoacclimation). Here, we have focused on the light-driven physiology of phytoplankton and how it impacts our interpretation of the satellite record. By advancing the description of photoacclimation, we have increased attribution of chlorophyll temporal anomalies to changes in mixed-layer light conditions, and consequently diminished attribution to other factors. Perhaps surprisingly, we find that biomass changes dominate chlorophyll anomalies in only a few restricted regions (Fig. 5a), but this result is in part a consequence of the MODIS time frame. During the earlier Sea-viewing Wide Field-of-view Sensor (SeaWiFS) mission, a major El Niño–La Niña transition was recorded, during which event biomass changes were a primary driver of chlorophyll variability[8].

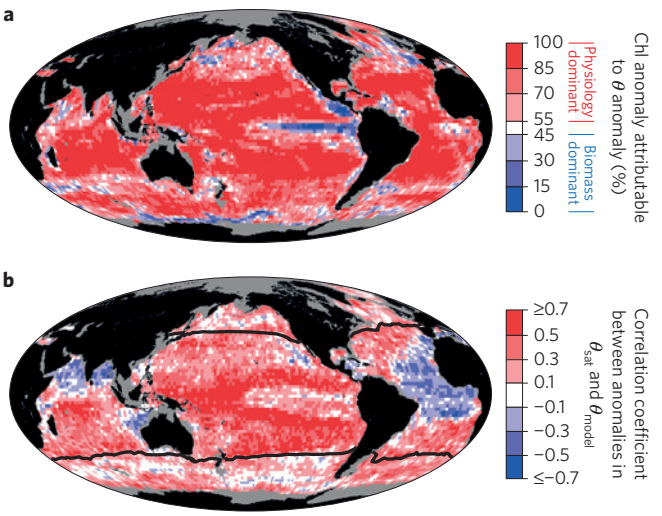

Figure 5 | Physiological contributions to global chlorophyll anomalies. **a**, Percentage of observed chlorophyll anomalies (that is, difference between monthly values for a given year and the average monthly value for the 11-year MODIS Aqua record (July 2002–January 2014)) that is accounted for by observed monthly anomalies in θ. **b**, Linear, least-squares correlation coefficients (r) between observed anomalies in θ and model-predicted θ anomalies attributed to photoacclimation (r values of ≥0.3 have mean p-value significance levels of <0.001). Black lines, annual mean SST of 15 °C, which approximately delineates the permanently stratified oceans from higher-latitude, seasonally deep-mixing regions[13]. Note that the large regions of negative correlations west of Africa and in the northern Indian Ocean (blue colours) correspond to regions with large atmospheric correction uncertainties for ocean retrievals.

Low-production central ocean gyres and high-latitude bloom-forming regions can have vastly different chlorophyll concentrations that reflect, to first order, differences in phytoplankton biomass driven by plankton predator–prey interactions[41] and mixed-layer nutrient loading[7]. However, a central message from the present investigation is that physiological factors must always be considered when evaluating chlorophyll data, particularly in the interpretation of interannual chlorophyll anomalies. This conclusion raises the question, how are previously reported inverse relationships between chlorophyll and SST anomalies mechanistically linked to phytoplankton physiology? Part of the answer to this question is that SST changes are often linked to changes in surface-layer mixing. Changes in mixed-layer depth can alter the light level to which phytoplankton are photoacclimated and may or may not influence surface-layer nutrient concentrations[42]. Both of these mechanisms impact phytoplankton physiology, and thus θ. In the present study, we quantify the photoacclimation response but also show that other factors can dominate interannual anomalies in θ (Fig. 5b). A challenge for future studies is to disentangle the remaining unexplained θ variability into contributions from, for example, nutrient changes, physical advection[42], community composition, and satellite retrieval errors. Such a partitioning will significantly refine our understanding of ocean ecosystem responses to contemporary climate variability.

Phytoplankton inhabiting the surface ocean mixed layer have evolved a diverse set of physiological tools to negotiate their highly

variable growth environment. Photoacclimation is an essential component of this plasticity, and the continued mechanistic refinement of its description is critical not only for the interpretation of global chlorophyll changes, but also assessments of ocean productivity[27], organic carbon export from the surface ocean to depth[43], and performance evaluations of modern coupled ocean ecosystem models[44]. Accurate photoacclimation models are also requisite for quantifying phytoplankton photoprotection under supersaturing light (that is, nonphotochemical quenching), which is the dominant signal registered in satellite-retrieved chlorophyll fluorescence quantum yield data[45]. Here, we call new attention to the potential importance of dark exposure periods during deep mixing on regulatory mechanisms of photoacclimation. Recognition of PQ pool redox changes in the dark was fundamental to the development of our revised photoacclimation model. It might be further suggested that regulation of photoacclimation is one role of chlororespiration in eukaryotes, the function of which has been debated[23].

By accounting for the photoacclimation response, we can conclude that temporal anomalies in surface chlorophyll over-represent associated changes in mixed-layer productivity for the MODIS record. However, caution is needed when extrapolating this conclusion to water-column-integrated production or the potential impacts of future ocean warming. With respect to the former, a shallowing of the mixed layer can drive an increase in surface-layer photosynthesis, but simultaneously causes a proportional expansion in the light-limited phytoplankton population below the mixed layer. These coincident effects have counteracting impacts on depth-integrated production. With respect to future warming, it is important to remember that the satellite record captures global phytoplankton responses only to present changes in the surface ocean environment, which are not fully reflective of the multifaceted changes anticipated with upcoming climate change. Understanding the integrated ramifications of these future changes will require a comprehensive and multi-stressor assessment of plankton ecosystem responses and feedbacks[46].

Received 10 June 2015; accepted 22 September 2015; published online 26 October 2015

References

1. Irwin, A. J. & Oliver, M. J. Are ocean deserts getting larger? *Geophys. Res. Lett.* **36**, L18609 (2009).
2. McClain, C. R., Signorini, S. R. & Christian, J. R. Subtropical gyre variability observed by ocean-color satellites. *Deep-Sea Res. II* **51**, 281–301 (2004).
3. Polovina, J. J., Howell, E. A. & Abecassis, M. Ocean's least productive waters are expanding. *Geophys. Res. Lett.* **35**, 3618 (2008).
4. Behrenfeld, M. J. *et al*. Climate-driven trends in contemporary ocean productivity. *Nature* **444**, 752–755 (2006).
5. Behrenfeld, M. J., Halsey, K. & Milligan, A. Evolved physiological responses of phytoplankton to their integrated growth environment. *Phil. Trans. R. Soc. B* **363**, 2687–2703 (2008).
6. Martinez, E., Antoine, D., D'Ortenzio, F. & Gentili, B. Climate-driven basin-scale decadal oscillations of oceanic phytoplankton. *Science* **326**, 1253–1256 (2009).
7. Siegel, D. A. *et al*. Regional to global assessments of phytoplankton dynamics from the SeaWiFS mission. *Remote Sens. Environ.* **135**, 77–91 (2013).
8. Gregg, W. W., Casey, N. W. & McClain, C. R. Recent trends in global ocean chlorophyll. *Geophys. Res. Lett.* **32**, L03606 (2005).
9. Kahru, M., Kudela, R., Manzano-Sarabia, M. & Mitchell, B. G. Trends in primary production in the California Current detected with satellite data. *J. Geophys. Res.* **114**, C02004, 10340 (2009).
10. Boyce, D. G., Lewis, M. L. & Worm, B. Global phytoplankton decline over the past century. *Nature* **466**, 591–596 (2010).
11. Laws, E. A. & Bannister, T. T. Nutrient- and light-limited growth of *Thalassiosira fluviatilis* in continuous culture, with implications for phytoplankton growth in the ocean. *Limnol. Oceanogr.* **25**, 457–473 (1980).
12. Geider, R. J. Light and temperature dependence of the carbon to chlorophyll ratio in microalgae and cyanobacteria: Implications for physiology and growth of phytoplankton. *New Phytol.* **106**, 1–34 (1987).
13. Behrenfeld, M. J., Boss, E., Siegel, D. A. & Shea, D. M. Carbon-based ocean productivity and phytoplankton physiology from space. *Glob. Biogeochem. Cycles* **19**, GB1006 (2005).
14. Halsey, K. H. & Jones, B. M. Phytoplankton strategies for photosynthetic energy allocation. *Annu. Rev. Mar. Sci.* **7**, 265–297 (2015).
15. Escoubas, J. *et al*. Light intensity regulation of cab gene transcription is signaled by the redox state of the plastoquinone pool. *Proc. Natl Acad. Sci. USA* **92**, 10237–10241 (1995).
16. Durnford, D. G. & Falkowski, P. G. Chloroplast redox regulation of nuclear gene transcription during photoacclimation. *Photosynth. Res.* **53**, 229–241 (1997).
17. Oelze, M., Kandlbinder, A. & Dietz, K. Redox regulation and overreduction control in the photosynthesizing cell: Complexity in redox networks. *Biochim. Biophys.* **1780**, 1261–1272 (2008).
18. Pfannschmidt, T. & Yang, C. The hidden function of photosynthesis: A sensing system for environmental conditions that regulates plant acclimation responses. *Protoplasma* **249**, S125–S136 (2012).
19. Cooley, J., Howitt, C. & Vermaas, W. Succinate: Quinol oxidoreductases in the cyanobacterium *Synechocystis* sp. strain PCC 6803: Presence and function in metabolism and electron transport. *J. Bacteriol.* **182**, 714–722 (2000).
20. Behrenfeld, M. J. *et al*. Controls on tropical Pacific Ocean productivity revealed through nutrient stress diagnostics. *Nature* **442**, 1025–1028 (2006).
21. Behrenfeld, M. J. & Milligan, A. J. Photophysiological expressions of iron stress in phytoplankton. *Annu. Rev. Mar. Sci.* **5**, 217–246 (2013).
22. Fujiki, T., Hosaka, T., Kimoto, H., Ishimaru, T. & Saino, T. *In situ* observations of phytoplankton productivity by an underwater profiling buoy system: Use of fast repetition rate fluorometry. *Mar. Ecol. Prog. Ser.* **353**, 81–88 (2008).
23. Peltier, G. & Cournac, L. Chlororespiration. *Ann. Rev. Plant Biol.* **53**, 523–550 (2002).
24. Vermaas, W. F. J. *Encyclopedia of Life Sciences* (John Wiley, 2001).
25. Behrenfeld, M. J., Marañón, E., Siegel, D. A. & Hooker, S. B. A photoacclimation and nutrient based model of light-saturated photosynthesis for quantifying oceanic primary production. *Mar. Ecol. Prog. Ser.* **228**, 103–117 (2002).
26. MacIntyre, H. L., Kana, T. M., Anning, T. & Geider, R. J. Photoacclimation of photosynthesis irradiance response curves and photosynthetic pigments in microalgae and cyanobacteria. *J. Phycol.* **38**, 17–38 (2002).
27. Westberry, T. K., Behrenfeld, M. J., Siegel, D. A. & Boss, E. Carbon-based primary productivity modeling with vertically resolved photoacclimation. *Glob. Biogeochem. Cycles* **22**, GB2024 (2008).
28. Platt, T. & Sathyendranath, S. Estimators of primary production for interpretation of remotely sensed data on ocean color. *J. Geophys. Res.* **98**, 14561–14567 (1993).
29. Behrenfeld, M. J. & Falkowski, P. G. A consumer's guide to phytoplankton primary productivity models. *Limnol. Oceanogr.* **42**, 1479–1491 (1997).
30. Roesler, C. S. & Perry, M. J. *In situ* phytoplankton absorption, fluorescence emission, and particulate backscattering spectra determined from reflectance. *J. Geophys. Res.* **100**, 13279–13294 (1995).
31. Maritorena, S., Siegel, D. A. & Peterson, A. R. Optimization of a semianalytical ocean color model for global-scale applications. *Appl. Opt.* **41**, 2705–2714 (2002).
32. Lee, Z. P., Carder, K. L. & Arnone, R. A. Deriving inherent optical properties from water color: A multi-band quasi-analytical algorithm for optically deep waters. *Appl. Opt.* **41**, 5755–5772 (2002).
33. Huot, Y., Morel, A., Twardowski, M. S., Stramski, D. & Reynolds, R. A. Particle optical backscattering along a chlorophyll gradient in the upper layer of the eastern South Pacific Ocean. *Biogeoscience* **5**, 495–507 (2008).
34. Martinez-Vicente, V., Dall'olmo, G., Tarran, G., Boss, E. & Sathyendranath, S. Optical backscattering is correlated with phytoplankton carbon across the Atlantic Ocean. *Geophys. Res. Lett.* **40**, 1154–1158 (2013).
35. Graff, J. R., Milligan, A. J. & Behrenfeld, M. J. The measurement of phytoplankton biomass using flow-cytometric sorting and elemental analysis of carbon. *Limnol. Oceanogr. Method* **10**, 910–920 (2012).
36. Graff, J. R. *et al*. Analytical phytoplankton carbon measurements spanning diverse ecosystems. *Deep-Sea Res. I* **102**, 16–25 (2015).
37. Mitchell, B. G. & Kahru, M. Bio-optical algorithms for ADEOS-2 GLI. *J. Remote Sens. Soc. Jpn* **29**, 80–85 (2009).
38. Gregg, W. W. & Casey, N. W. Global and regional evaluation of the SeaWiFS chlorophyll data set. *Remote Sens. Environ.* **93**, 463–479 (2004).
39. Westberry, T. K., Boss, E. & Lee, Z. The influence of Raman scattering on ocean color inversion models. *Appl. Opt.* **52**, 5552–5561 (2013).
40. Henson, S. A. *et al*. Detection of anthropogenic climate change in satellite records of ocean chlorophyll and productivity. *Biogeoscience* **7**, 621–640 (2010).
41. Behrenfeld, M. J. Climate-mediated dance of the plankton. *Nature Clim. Change* **4**, 880–887 (2014).

42. Lozier, M. S., Dave, A. C., Palter, J. B., Gerber, L. M. & Barber, R. T. On the relationship between stratification and primary productivity in the North Atlantic. *Geophys. Res. Lett.* **38**, L18609 (2011).
43. Siegel, D. A. *et al*. Global assessment of ocean carbon export using food-web models and satellite observations. *Glob. Biogeochem. Cycles* **28**, 181–196 (2014).
44. Doney, S. C. *et al*. Skill metrics for confronting global upper ocean ecosystem-biogeochemistry models against field and remote sensing data. *J. Mar. Syst.* **76**, 95–112 (2009).
45. Behrenfeld, M. J. *et al*. Satellite-detected fluorescence reveals global physiology of ocean phytoplankton. *Biogeoscience* **6**, 779–794 (2009).
46. Boyd, P. W., Lennartz, S. T., Glover, D. M. & Doney, S. C. Biological ramifications of climate-change-mediated oceanic multi-stressors. *Nature Clim. Change* **5**, 71–79 (2015).
47. Halsey, K. H., Milligan, A. J. & Behrenfeld, M. J. Contrasting strategies of photosynthetic energy utilization drive lifestyle strategies in ecologically important picoeukaryotes. *Metabolites* **4**, 260–280 (2014).

Acknowledgements
This work was supported by the National Aeronautics and Space Administration's Ocean Biology and Biogeochemistry Program.

Author contributions
M.J.B. designed the study; M.J.B., R.T.O'M. and E.S.B. conducted satellite data analyses and photoacclimation model development; M.J.B. and R.T.O'M. prepared display items; M.J.B. wrote the manuscript with contributions from all authors.

Additional information
Supplementary information is available in the online version of the paper. Reprints and permissions information is available online at www.nature.com/reprints. Correspondence and requests for materials should be addressed to M.J.B.

Competing financial interests
The authors declare no competing financial interests.

nature climate change

SUPPLEMENTARY INFORMATION

DOI: 10.1038/NCLIMATE2838

Revaluating ocean warming impacts on global phytoplankton

SUPPLEMENTARY DISCUSSION

1. Expanded Description of Photoacclimation Physiology

In the current evaluation of photoacclimation in natural mixed layer phytoplankton communities, we have called attention to the role of PQ pool redox state sensing. The regulation of photoacclimation has been investigated extensively and involves multiple feedbacks. Laboratory studies have demonstrated that PQ pool redox state influences transcription rates for multiple genes, both photosynthetic and non-photosynthetic (Pfannschmidt and Yang 2012). Transcript levels for light harvesting complex proteins (LHC's) decrease when the PQ pool is reduced either by exposure to high light or when artificially reduced under low-light conditions through the application of the electron transport inhibitor, 2,5-Dibromo-6-isopropyl-3-methyl-1,4-benzoquinone (DBMIB) (Escoubas et al. 1995, Chen et al. 2004). Production of the major components of the two photosystems is also altered by high-light or low-light plus inhibitor induced changes in PQ redox state, with PQ pool reduction favoring up-regulation of PSI genes and oxidation favoring up-regulation of PSII (Pfannschmidt et al. 1999). These findings indicate that sensing of the PQ pool redox state is an important aspect of tuning light harvesting machinery in response to changing light conditions. Furthermore, while equivalent responses to PQ reduction in the dark remain to be tested directly, the observed synonymous effect of high-light and inhibitor-plus-low-light treatments suggests that regulation by PQ pool redox sensing functions in a manner independent of how the PQ pool is reduced.

Regulation of mRNA levels by PQ redox sensing, however, is only one of the mechanisms involved in photoacclimation. Concentrations of mRNA for photosynthetic

genes can be transient (McKim & Durnford 2006) and decorrelated from actual protein concentrations (Lefebvre et al. 2010). Post-transcriptional processes thus play an additional role in long-term photoacclimation (Durnford et al. 2003, see Wobbe 2008 for review). Importantly, PQ redox state has been shown to influence photoacclimation through post-transcriptional processes, as mutants with chronically reduced PQ pools possess minimal light harvesting antennas without changes in antenna transcript concentrations (Frigerio et al. 2007). In addition to PQ pool redox state, other signals are used by photosynthetic organism to monitor their light environment and regulate photosynthetic gene expression, such as thioredoxin production (Stenbaek and Jensen 2010), sensing of the transthylakoid pH gradient (Chen et al. 2004), and hydrogen peroxide concentrations (Vandenabeele et al. 2004). For simplicity, we focus in the main manuscript on PQ redox sensing, but recognize here that the mechanisms of photoacclimation are complex and can involve multiple light-sensing signals that co-vary with the reduction state of the PQ pool.

Another aspect of photoacclimation that is emerging as an important regulatory mechanism is the role of the gun4 protein. Gun4 stimulates the activity of Mg-chelatase, which is an enzyme that catalyzes the first committed step of chlorophyll biosynthesis. Mutants lacking gun4 exhibit decreased chlorophyll synthesis and decreased expression of nuclear-encoded photosynthetic genes (Mochizuki et al. 2000, Brzezowski et al. 2014). Thus, gun4 appears to function in retrograde signaling from the chloroplast to the nucleus, but the underlying mechanisms remain obscure. However, proper complexing of gun4 with Mg-chelatase does require reduction of a disulfide bridge by chloroplast thioredoxin (Luo et al 2012), which in turn is activated by reduced ferredoxin. As thioredoxin and

ferredoxin levels are linked to photosynthetic electron flow, it may again be expected that gene expression due to gun4 may correlate with PQ redox state.

2. Global Data Sets

Ocean satellite data used in our analysis are from the MODerate resolution Imaging Spectroradiometer on Aqua (MODIS Aqua, July 2002 to January 2014). Standard Level 3 products at ~9 km (1/12 of a degree) spatial resolution for chlorophyll concentration, photosynthetically active radiation (*PAR*) (see **Table of Notation, Section 5**), and the diffuse attenuation coefficient at 490 nm (K_{490}) were acquired from http://oceancolor.gsfc.nasa.gov/cms/. Diffuse attenuation coefficients for *PAR* (K_d) were calculated from K_{490} following Morel et al. (2007): $K_d = 0.0665 + 0.874\ K_{490} - 0.00121/\ K_{490}$. Phytoplankton carbon concentrations were estimated from particulate backscatter coefficients (b_{bp}) following Westberry et al. (2008) and based on MODIS Aqua b_{bp} values from the Garver-Siegel-Maritorena inversion method (Maritorena et al., 2002) and archived by the Ocean Color MEaSUREs project at UCSB (http://wiki.icess.ucsb.edu/measures/Main_Page). Day length values were calculated as a function of date and latitude following Kirk (1994). Mixed layer depth (*MLD*) values were calculated from salinity, temperature and pressure data converted to density (sigma-theta) and based on daily HYCOM multi-layer global models (source: https://hycom.org/). All final global data products used in our analysis are available through http://www.science.oregonstate.edu/ocean.productivity. Global data were aggregated into 2^o latitude x 2^o longitude bins for the analysis of chlorophyll variability shown in **figure 5** of the main manuscript.

3. Photoacclimation Model

3.1 *Model narrative*

A wide range of factors influence the carbon-to-chlorophyll ratio (θ) (see **Table of Notation, Section 5**) of natural mixed-layer phytoplankton populations, including light conditions, nutrient limitation of division rate (Laws & Bannister 1980, Smith & Gieder 1985, Sunda & Huntsman 1995, Halsey & Jones 2015), unique responses to particular nutrient stressors such as iron (Behrenfeld et al. 2006, Schrader et al. 2011, Behrenfeld & Milligan 2012), and various taxon-specific factors (e.g., importance of accessory photosynthetic pigments) (Sunda & Huntsman 1995, MacIntyre et al. 2002, Halsey et al. 2014). In addition, the rate of change in mixed layer growth conditions relative to the rate of change in physiological state is important in determining whether or not observed values of θ represent steady-state solutions (Cullen & Lewis 1988). For the current study, the objective of our modeling analysis was focused exclusively on characterizing steady-state solutions for light-driven changes in θ in response to changes in PAR, K_d, and MLD (i.e., photoacclimation). We attribute differences between model predications of θ and observed values to the multitude of other factors noted above that impact cellular chlorophyll levels.

In the main text and in Supplemental Section 1, we call attention to the potential importance of PQ pool reduction in the dark for regulating photoacclimation. Recognition of this phenomenon was fundamental to our model development because it implied that dark regions of the mixed layer have little impact on θ, thereby refocussing our attention solely on properties of the photic layer. Despite the importance of this

insight, the model described here does not explicitly quantify PQ redox states of the mixed layer. Instead, the model evaluates the tuning of θ to changes in photosynthesis that result from variability in *PAR* and K_d (day length was not considered as a primary driver of θ variability (Verity 1981, Tang & Vincent 2000), since for a given value of θ changes in daylength do not alter the fraction of the photoperiod during which the PQ pool is oxidized versus reduced). Model solutions for deep-mixing conditions are then modified as a function of the median mixed layer light level for shallow mixing conditions, thereby retaining the earlier view regarding the utility of this property as an index of the balancing point between 'on' and 'off' signals for chlorophyll synthesis within the photic zone.

To evaluate θ solutions for deep mixing, the model calculates time- and depth-resolved mixed layer light levels for a globally-representative range of *PAR* and K_d. Photosynthesis is calculated as a saturating function of submarine light intensity, where α is the light-limited initial slope of this relationship and P_{max} is the light-saturated maximum rate. A change in θ from photoacclimation results in a change in α (MacIntyre et al. 2002), which consequently impacts the light level at which photosynthesis saturates. This saturation light level is characterized by the index, $E_k = P_{max} / \alpha$. To execute the model, a value for E_k must first be assigned to one specific light environment, which we refer to as the baseline 'bright' mixed layer. This baseline was taken as the condition of $K_d = 0.025$ m^{-1} and *PAR* = 4 moles photon m^{-2} h^{-1} (equivalent to a noon irradiance of 1800 μmole photon m^{-2} s^{-1}), for which E_k was assigned a value of 400 μmole photon m^{-2} s^{-1}. The photoacclimation response was then determined based

upon *NPP* for all other combinations of *PAR* and K_d relative to *NPP* for this baseline condition (NPP_{bright}).

The above approach was used because the model was intended to characterize θ variability due to photoacclimation-based changes in E_k alone, and not the influence of other factors impacting the absolute value of *NPP* (e.g., biomass, nutrient availability, taxonomic composition of the phytoplankton assemblage, temperature). Accordingly, an arbitrary value for P_{max} can be chosen that is then applied to all modeled light conditions (we used, P_{max} = 1 mg C m^{-3} h^{-1}). We then adjust E_k (which is proportional to a change in θ in the model) for each combination of *PAR* and K_d such that the associated rate of *NPP* relative to NPP_{bright} follows a relationship (**Fig. S1**) consistent with laboratory observations (e.g., **Fig. 1D** in main manuscript).

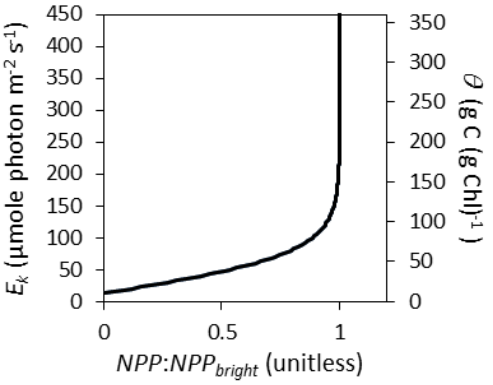

Figure S1. Model relationship between relative net primary production (NPP:NPP_{bright}) and (left) E_k and (right) θ.

The key outcome of our modelling analysis is that photoacclimation under deep mixing conditions results in E_k variability (and thus light-driven changes in θ) that can be described as a simple function of $PAR^{0.45}/ K_d$. This deep mixing solution is then adjusted for mixing shallower than 6 optical depths based on a median mixed layer light level (I_{ML}) relationship described by Behrenfeld et al. (2002, 2005) and Westberry et al. (2008). This shallow mixing correction ranges from a factor of 1 to 1.8 for mixing of 6 to 0 optical depths.

As noted at the beginning of this section, a variety of factors impact observed values of θ in natural phytoplankton populations. However, our model is focused only on θ variability due to photoacclimation, through its impacts on E_k. To apply our model results to satellite data, a proportionality factor is applied to account for the average impact of these other factors on θ. This scalar was determined by first plotting MODIS satellite θ data against model-based predictions of E_k. This comparison yielded a coefficient of determination (r^2) of 0.92 (as in **Fig. 3c** of the main manuscript) and a regression slope of 0.8 g C m^2 h (g Chl µmol photon) $^{-1}$. The slope of this relationship (i.e., 0.8) provides the necessary E_k –to- θ proportionality factor. While global θ variability observed from space registers a diversity of physiological responses (as discussed above), it can be noted for context that an E_k –to- θ conversion factor of 0.8 g C m^2 h (g Chl µmol photon) $^{-1}$ corresponds to the average conversion factor for steady state division rates of 0.4 d^{-1} based on observations of Halsey et al. (2014) for cultures of the diatom, *Thalassiosira weisflogii*, the chlorophyte, *Dunaliella tertiolecta*, and the two cosmopolitan picoeukaryotes, *Ostreococcus tauri* and *Micromonas pusilla*.

3.2 *Analytical description*

As described in the preceding section, our revised description of photoacclimation derives from a time- and depth-resolved model that determines the steady-state value for E_k based on a fixed relationship between E_k and relative net primary production (*NPP*) (**Fig. S1**). Photosynthesis is described as a saturating function of submarine irradiance (*E(t,z)*, µmole photon m^{-2} s^{-1}) following Jassby and Platt (1976) and then integrated over time and depth of the photic zone *(ΣNPP)*:

$$\Sigma NPP = P_{max} \int_{Zeu}^{0} \int_{0}^{24hr} tanh\left(\frac{E(t,z)}{E_k}\right) dtdz \, . \quad \text{(S1)}$$

where: Z_{eu} = depth at which the photosynthetic rate is 0.01 µg C m^{-3} h^{-1}, $E(t,z) = iPAR(t)e^{-K_d z}$, $iPAR(t)$ = incident sunlight (µmole photon m^{-2} s^{-1}) at time, t, just below the ocean surface, and respiration is assumed proportional to ΣNPP and independent of deep mixing below Z_{eu}. The relationship between E_k and ΣNPP (**Fig. S1**) is described by:

$$E_k = 50\, atanh\left(\frac{\Sigma NPP}{c_3 P_{max} DL}\right) + 10 \quad \text{(S2)}$$

where the two constants (50 and 10) have units of µmole photon m^{-2} s^{-1} and DL is the length of the photoperiod in hours (see Section *3.3 Sensitivity Analysis*). c_3 has a value of 68 m and is the ratio $\Sigma NPP/(P_{max}\, DL)$ for the baseline 'bright mixed layer' condition of K_d = 0.025 m^{-1}, PAR = 4 mole photon m^{-2} h^{-1}, and E_k = 400 µmole photon m^{-2} s^{-1} (see previous section).

Equations S1 and S2 represent two equations with two unknowns ($\Sigma NPP/P_{max}$ and E_k) and hence are solvable, provided a model for temporal changes in $iPAR(t)$ and Z_{eu}. Changes in $iPAR(t)$ over the photoperiod were described as:

$$iPAR(t) = iPAR_{noon} \sin\left(\pi\, (t - t_{sr})/DL\right), \quad \text{(S3)}$$

where t_{sr} is the time of sunrise in hours and $t_{sr} + DL > t \geq t_{sr}$. Integrating S3 over time and dividing by photoperiod gives the value of PAR (mole photon m^{-2} h^{-1}):

$$PAR = \frac{0.0036}{DL}\int_{t_{sr}}^{t_{sr}+DL} iPAR_{noon} sin\left(\frac{\pi}{DL}(t - t_{sr})\right) dt = \frac{0.0072}{\pi} iPAR_{noon} \quad \text{(S4)}$$

$$\rightarrow iPAR_{noon} = \frac{\pi PAR}{0.0072}$$

where the 0.0036 factor provides a conversion from μmole s^{-1} to mole h^{-1}. Substituting into the irradiance equation (S4) and performing a time shift, $t = t - t_{sr}$:

$$E(t,z) = iPAR_{noon} sin\left(\frac{\pi}{DL}t\right) e^{-K_d z}, \qquad DL \geq t \geq 0 \text{ (it is 0 otherwise).} \quad \text{(S5)}$$

To solve for E_k , we look for the root of:

$$\frac{1}{DL}\int_{Z_{eu}}^{0}\int_{0}^{DL} tanh\left(\frac{iPAR_{noon} sin\left(\frac{\pi}{DL}t\right) e^{-K_d z}}{E_k}\right) dt dz - c_3\, tanh\left(\frac{E_k - 10}{50}\right) = 0 \quad \text{(S6)}$$

which was evaluated using Matlab's 'fminbnd' algorithm with bounds for E_k of 0 and 450 μmole photon m^{-2} s^{-1}. Z_{eu} is iteratively computed as the depth at which $NPP = 0.01$ μg C m^{-3} h^{-1}:

$$P_{max} tanh\left(\frac{E(t,z_{eu})}{E_k}\right) = 0.01 \rightarrow E(t,z_{eu}) = E_k atanh(0.01/P_{max}), \quad \text{(S7)}$$

$$\rightarrow tanh\left(\frac{iPAR_{noon} sin\left(\frac{\pi}{DL}t\right) e^{-K_d z_{eu}}}{E_k}\right) = \frac{0.01}{P_{max}} \rightarrow Z_{eu}(t)$$

$$= -\frac{1}{k_d} ln\left\{\frac{E_k atanh^{-1}(0.01/P_{max})}{iPAR_{noon} sin\left(\frac{\pi}{DL}t\right)}\right\}$$

The solution for S6 yields predicted steady-state E_k values for any given combination of K_d and PAR. For values of PAR ranging from 0.2 to 4.5 moles photons m^{-2} h^{-1} and K_d ranging from 0.025 to 2.1 m^{-1}, we find that these solutions for E_k collapse upon a single relationship with $PAR^{0.45}$ / K_d under conditions of $MLD > Z_{eu}$ (**Fig. S2**). Applying the E_k –to-θ proportionality factor of 0.8 described above, this relationship gives the deep-mixing solution for θ (θ_{DM}; equation 2 of the main text):

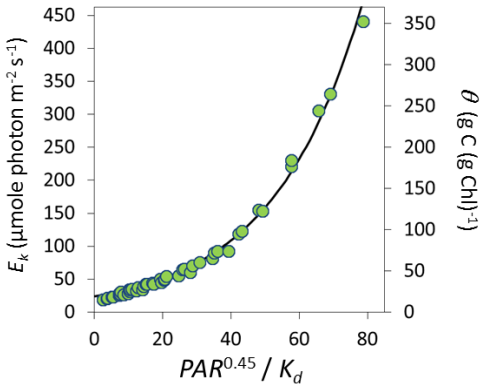

Figure S2. Model-based relationship between $PAR^{0.45}/K_d$ and (left) E_k and (right) θ. x-axis units: PAR = moles photons m^{-2} h^{-1} and K_d = m^{-1}

$$\theta_{DM} = c_1 \, e^{c_2 \, PAR^{0.45}/K_d} \qquad \text{(S8)}$$

where c_1 = 19 g C (g Chl)$^{-1}$ and c_2 = 0.038 m^{-1}.

For conditions of shallow mixing, taken as MLD < 6 optical depths (approximate depth of Z_{eu} = 0.01 µg C m^{-3} h^{-1}), θ_{DM} was adjusted upward using a published relationship derived from field observations and satellite data (Behrenfeld et al 2002, 2005, Westberry et al. 2008):

$$Chl{:}C = \theta^{-1} = c_4 + c_4 \, e^{-3 I_{ML}} \qquad \text{(S9)}$$

where $I_{ML} = PAR \times e^{-0.5 \, Kd \times MLD}$ and the parameter in the exponent (i.e., 3) has units of m^2 h (mole photon)$^{-1}$. Assigning a value for c_4 = 1 gC (gChl)$^{-1}$, this shallow mixing

correction ($\Delta\theta_{SM}$) is the ratio of the solution for S9 at 6 optical depths ($= 1 + e^{-3I_{ML}} = 1 + e^{-3\,PAR\,e^{-0.5\times6}} = 1 + e^{-0.15\,PAR}$) over the solution for S9 at *MLD*:

$$\Delta\theta_{SM} = \frac{1+e^{-0.15\,PAR}}{1+e^{-3\,I_{ML}}} \qquad \text{(S10)}$$

Example values for $\Delta\theta_{SM}$ from equation S10 are shown in **figure S3** for optical mixing depths ≤ 6 and a range of *PAR* values. For mixing depths greater than 6 optical depths, $\Delta\theta_{SM}$ is assigned a value of 1.

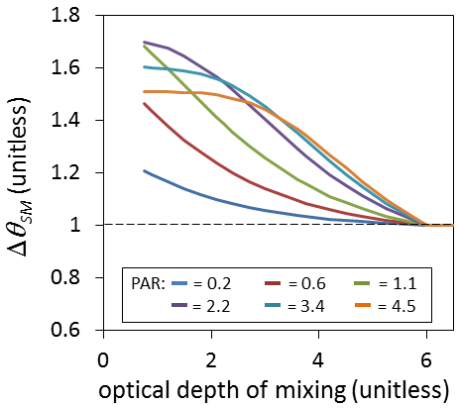

Figure S3. Relationship between $\Delta\theta_{SM}$ and optical depth of mixing for a range of *PAR* values (inset legend)

3.3 *Sensitivity analysis*

The model described in Sections 3.1 and 3.2 predicts steady state photoacclimation states for mixed layer phytoplankton over a wide range of *PAR*, K_d, and *MLD* values by finding values for E_k that follow a predefined relationship with ΣNPP (Eq. S2, **Fig. S1**). This relationship employs 2 parameters, a minimum value for E_k of 10 µmole photon m^{-2} s^{-1} and a midpoint value for E_k of 50 µmole photon m^{-2} s^{-1} where ΣNPP is 0.5 ΣNPP_{bright}. These parameter values were taken as representative for natural phytoplankton populations, but measured values can exhibit significant variability between species (Falkowski et al. 1985, MacIntyre et al. 2002). Sensitivity tests were thus conducted to evaluate how model predictions of E_k change from our baseline results for modified values of the minimum E_k and midpoint E_k parameters (**Fig. S4**). This evaluation shows that an increase in the minimum E_k from 10 to 25 µmole photon m^{-2} s^{-1}

has a negligible impact on model predictions across all deep mixing scenarios and that even an increase to 60 µmole photon m^{-2} s^{-1} has only a minor effect at the lowest predicted values of E_k (**Fig. S4a**). Similarly, both a doubling and a halving of the midpoint value for E_k has little impact on model predictions compared to the baseline parameterization (**Fig. S4b**). These results thus indicate that the model predictions are relatively robust to our choice of parameter values for the E_k versus ΣNPP relationship.

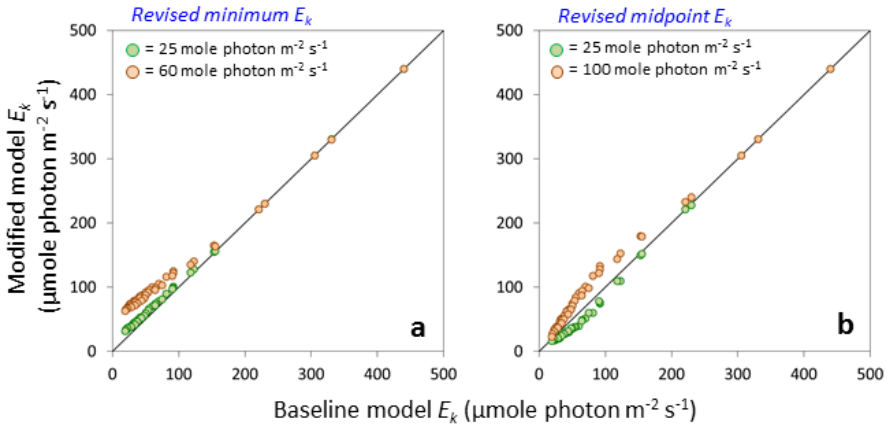

Figure S4. Comparison of E_k predictions for the baseline model parameterization and modified values for the (a) minimum E_k and (b) midpoint E_k.

The model also employs a shallow mixing correction ($\Delta\theta_{SM}$) for conditions of MLD < 6 optical depths that derives from earlier field and satellite studies (Eq. S9). The sensitivity of our results to this characterization of $\Delta\theta_{SM}$ can be evaluated by comparing satellite θ data and model predictions with and without the shallow mixing correction. The result of this comparison is that, for the global data set, the coefficient of determination (r^2) between model and observed θ decreases from $r^2 = 0.92$ for the full model (**Fig. 3c** in main manuscript) to $r^2 = 0.91$ for the deep solution only (i.e., θ_{DM}). Thus, our conclusion that photoacclimation is a significant driver of satellite-observed θ variability is robust to uncertainties in this shallow mixing correction. The reason for this result is that the magnitude of $\Delta\theta_{SM}$ tends to covary with θ_{DM}. More specifically, shallow mixing conditions at higher latitudes are often found during late summer when PAR is

near maximal and phytoplankton biomass (thus, K_d) is low. Shallow mixing environments are also found at lower latitudes (e.g., central ocean gyres) where *PAR* tends to be high and K_d tends to be low. Consequently, these regions (times) where the $\Delta\theta_{SM}$ adjustment is significant also correspond to regions (times) when the deep-mixing model solution gives elevated values for θ_{DM}.

While the correlation between modeled and measured θ is insensitive to the $\Delta\theta_{SM}$ adjustment at the global scale, the significance of this correction becomes apparent by focusing on specific ocean regions where the dynamic range in θ is more constrained. This effect is perhaps best illustrated by regions where *MLD* varies seasonally from > Z_{eu} to < Z_{eu}. For example, **Figure S5** shows model predictions and satellite retrievals of θ over the MODIS record for the North Atlantic L2 chlorophyll variance bin (see **Fig. 3a** of main manuscript). With the $\Delta\theta_{SM}$ correction included, the timing and amplitude of the θ seasonal cycle is very similar between the modeled and observed data (**Fig. S5a**). In contrast, the seasonal cycle for θ_{DM} exhibits a similar seasonal pattern as the satellite data, but model values underestimate observed values during the summer when mixing depths are shallower than Z_{eu} (**Fig. S5b**).

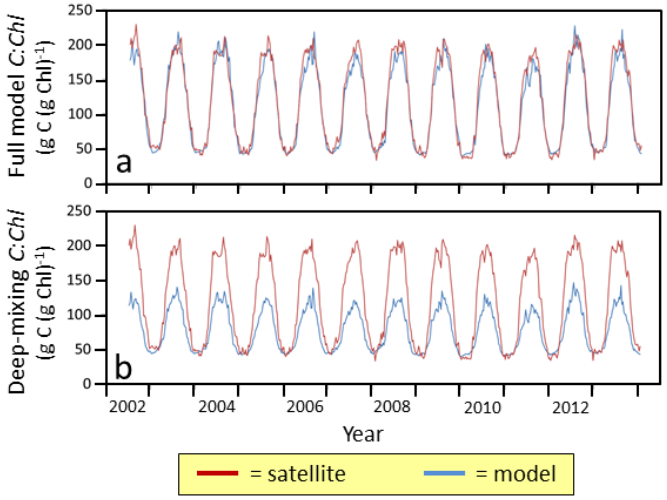

Figure S5. Model predictions and satellite retrievals of θ for the North Atlantic L2 chlorophyll variance bin. (a) Model values with a shallow mixing correction. (b) Model values without a shallow mixing correction.

3.4 *Comparison with field data*

The current study is focused on the contribution of photoacclimation to satellite observed global variability in mixed layer θ. Future studies comparing model predictions to field data will allow further testing and refinement of the new photoacclimation relationship. To this end, we describe here an initial evaluation of model performance using field data. A more extensive evaluation is currently being prepared as a separate manuscript (Silsbe et al 2015).

Direct measurements of θ in the field are uncommon due the challenge of separating phytoplankton cells from other particulate organic forms (Graff et al. 2015). Nevertheless, the sustained measurements conducted as part of the Hawaii Ocean Time-series (HOT) program provide a means for, at least qualitatively, testing our photoacclimation model. Seasonal changes in mixed layer chlorophyll concentrations and chlorophyll-specific ^{14}C uptake (P^b_{opt}) at HOT have been shown to largely reflect variability in θ (Letelier et al. 1993, Winn et al. 1995, Behrenfeld & Boss 2003, Chavez et al. 2011). Using HOT data compiled by Behrenfeld and Boss (2003) for the period 1991 to 1999, we compared field measured P^b_{opt} data with predicted values of θ based on our photoacclimation model (**Fig. S6a**). This comparison shows remarkable correspondence ($r^2 = 0.54$) between these two properties given that model θ values only consider contributions from photoacclimation while additional factors can influence variability in P^b_{opt}.

A second historical long-term data set available for testing our model comes from the Bermuda Atlantic Time Series (BATS) program. In contrast to the HOT site, the annual cycle in chlorophyll at the BATS site is, to first order, dominated by an annual bloom in biomass (Chavez et al. 2011). However, for the period 1991 to 1996, the BATS program included sustained measurements of *Prochlorococcus* chlorophyll fluorescence per cell ($F_{Pro}/cell$) (Durand et al. 2001), which thus tracks the biomass-independent component of chlorophyll variability. Taking the inverse of $F_{Pro}/cell$ as a proxy of θ, a comparison can therefore be made between these data and our model predictions of the photoacclimation response. The result of this comparison shows an excellent correspondence ($r^2 = 0.64$) in seasonal cycles for the two properties (**Fig. S6b**). Again, an exact correspondence between the model and field results is not anticipated since the model predicts light-driven θ variability for mixed phytoplankton assemblages, while

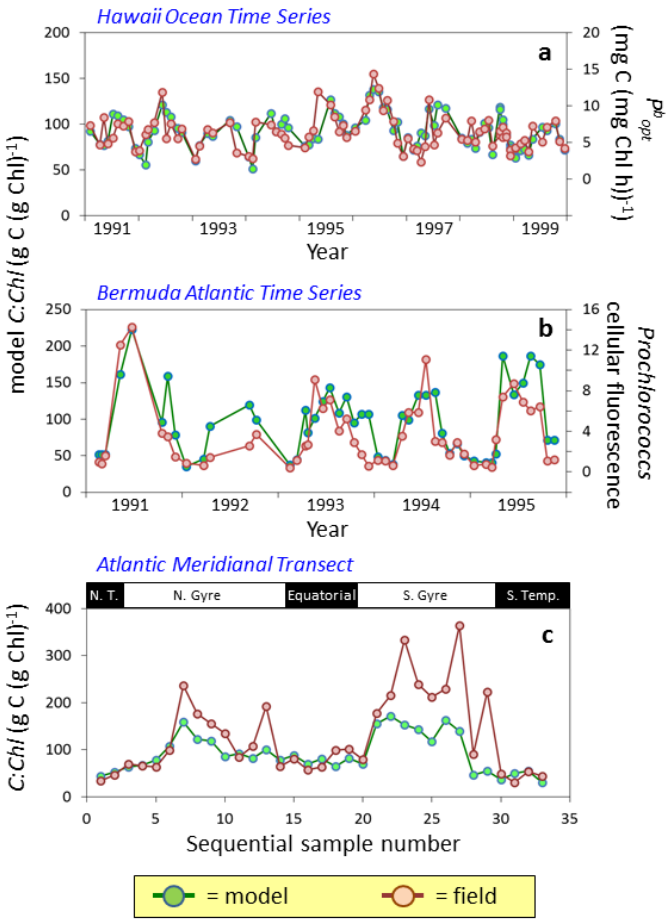

Figure S6. Comparison of model θ estimates and field measurements of (a) P^b_{opt} (from Behrenfeld and Boss 2003), (b) *Prochlorococcus* fluorescence per cell (from Durand et al. 2001) and (c) θ (from Graff et al. 2015).

$F_{Pro}/cell$ is a species-specific property that includes responses to other factors influencing cellular pigmentation (e.g., nutrient stress).

In the recent study of Graff et al. (2015), analytical measurements of phytoplankton carbon and chlorophyll were reported from the 10 October to 24 November 2012 Atlantic Meridional Transect (AMT-22), with samples spanning from roughly 45^o N to 45^o S latitude. These measurements provide the first direct field assessments of phytoplankton θ for comparison with our photoacclimation model predictions. Results of this comparison show consistent latitudinal patterns for modeled and measured θ values (**Fig. S6c**), with an overall coefficient of determination of r^2 = 0.64. The largest deviations between field and model data are observed in the central gyres of the north and south Atlantic, consistent with the expectation of elevated nutrient stress in these waters.

As a separate study, Silsbe et al. (2015) have evaluated the performance of our photoacclimation model through comparisons with field-based ^{14}C uptake measurements (Huot et al. 2007) of E_k conducted during the 26 October to 11 December 2004 Biogeochemistry and Optics South Pacific Experiment (BIOSOPE). BIOSOPE measurements spanned from 8^o to 35^o S latitude and from 72^o to 141^o W longitude. Silsbe et al. (2015) observed a significant correspondence between measured and model E_k for the BIOSOPE data set (r^2 = 0.7, slope = 0.9, $p<0.01$, n = 198). Taken together, the findings of Silsbe et al. and the results shown in **figure S6** indicate that the model developed during the current study effectively captures photoacclimation responses in natural mixed layer phytoplankton populations.

3.5 *Comparison to previous model*

Satellite retrievals of phytoplankton carbon (*C*) and chlorophyll (*Chl*) have previously been employed to estimate global ocean *NPP* using a model referred to as the Carbon-based Productivity Model (CbPM) (Behrenfeld et al 2005, Westberry et al. 2008). The CbPM partitions *Chl:C* variability into components of photoacclimation and nutrient stress. The photoacclimation relationship was based on the field study of Behrenfeld et al (2002), but modified such that light-driven changes in *Chl:C* were expressed as a function of the median mixed layer light level (I_{ML}) and parameterized such that the relationship enveloped ~99% of the satellite *Chl:C* data. Differences between this photoacclimation relationship and observed *Chl:C* values were then taken as a measure of nutrient stress and used to proportionately reduced modeled phytoplankton division rates from an assigned maximum potential rate of 2 divisions per day.

The CbPM photoacclimation relationship yielded good correlations with observed *Chl:C* variability within regional chlorophyll variance bins (similar to those shown in **Fig. 3a** of the current manuscript), particularly for bins within the permanently stratified ocean (Behrenfeld et al 2005). However, these relationships differed significantly between bins (as would be expected from the relationships shown in **Fig. 3b** of the current manuscript). Accordingly, the CbPM relationship attributes very little θ variability to photoacclimation, which can be illustrated by converting CbPM estimates of light-driven *Chl:C* variability into values of θ (i.e., $\theta = Chl{:}C^{-1}$) (**Fig. S7a**). The vast majority of θ variability unexplained by the CbPM photoacclimation term is thus assigned to nutrient-driven variability in phytoplankton division rates.

In contrast to the CbPM relationship, the current study ascribes a far greater fraction of θ variability to photoacclimation (**Fig. 3c** (main manuscript), **Fig. S7b**). However, while this photoacclimation response accounts for 92% of the observed global θ data, scatter around this relationship still allows for considerable residual θ variability attributable to other factors, such as nutrient stress, taxonomy, temperature, etc. The contribution of these other factors is reflected by the range in observed θ values for any given modeled value for the photoacclimation effect (e.g., vertical red line in **Fig. S7b**). Partitioning this remaining variability into its contributing components represents one of the important new challenges for future interpretations of the satellite record.

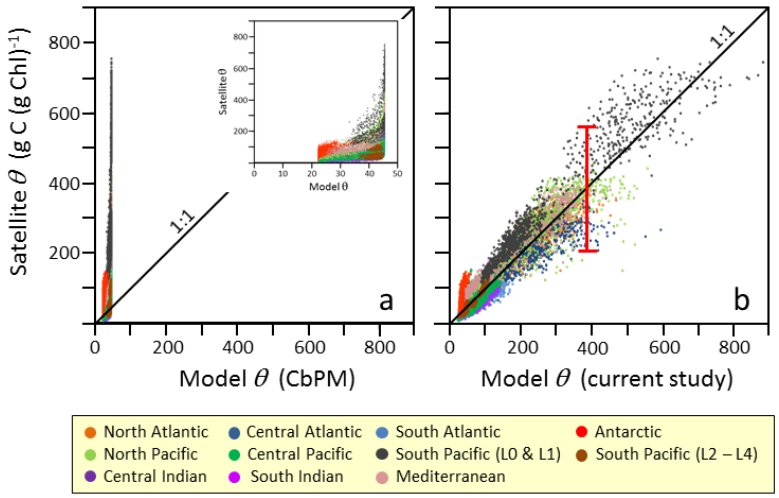

Figure S7. Satellite observed θ versus model estimates of θ variability due to photoacclimation for (a) the CbPM and (b) the current model. The inset figure in panel (a) shows results with an x-axis range of only 0 to 50 g C (g Chl)$^{-1}$.

4. Satellite θ time-series for all regional bins

Figure 4 of the main manuscript shows 11 examples of satellite- and model-based time-series of θ for the MODIS record. On the following page, **figure S8** shows the satellite and model θ time-series for all 37 regional bins.

▼ **Figure S8** (next page). Observed (red line) and model (blue line) time series of θ for our 37 regional bins (see main manuscript **Fig. 3a** for bin map and designations). Panels are oriented from left to right by chlorophyll variance level (increasing variance to right), and from top to bottom by ocean basin.

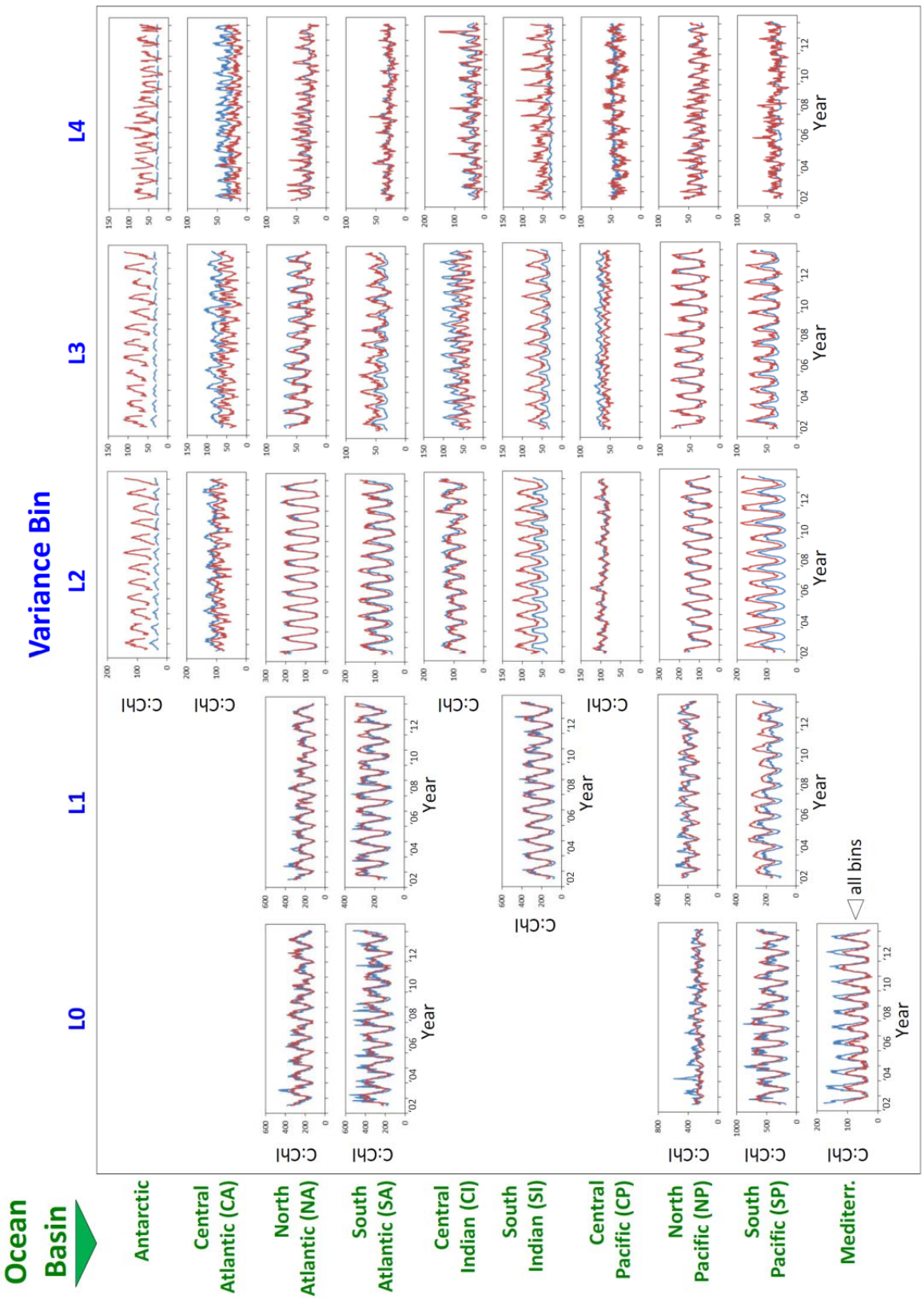

5. Table of notation used in Supplemental Information

Variable	Name	Units
α	Light-limited initial slope of photosynthesis	μg C m^{-1} μmol $photon^{-1}$
θ	Carbon-to-chlorophyll	g C (g Chl)$^{-1}$
θ_{DM}	Carbon-to-chlorophyll in deep mixing case	g C (g Chl)$^{-1}$
$\Delta\theta_{SM}$	Carbon-to-chlorophyll adjustment for shallow mixing	unitless
PAR	Average diurnal downwelling photosynthetic radiation	mol photon m^{-2} h^{-1}
iPAR	Instantaneous downwelling photosynthetic radiation	μmol photon m^{-2} s^{-1}
$iPAR_{noon}$	*iPAR* value at noon	μmol photon m^{-2} h^{-1}
E_k	Light saturation index	μmol photon m^{-2} h^{-1}
E	Irradiance	μmol photon m^{-2} h^{-1}
I_{ML}	Median mixed layer irradiance	μmol photon m^{-2} h^{-1}
t	Time	h
DL	Day length	h
K_d	Diffuse attenuation coefficient for *PAR*	m^{-1}
ΣNPP	Euphotic depth integrated daily photosynthesis	mg C m^{-2}
NPP	Net photosynthesis	mg C m^{-3} h^{-1}
NPP_{bright}	Net photosynthesis under bright conditions (*PAR* = 4 mol m^{-2} h^{-1}, K_d = 0.025m^{-1})	mg C m^{-3} h^{-1}
P_{max}	Light saturated rate of photosynthesis	μg C m^{-3} h^{-1}
c_1	Constant	19 g C (g Chl)$^{-1}$
c_2	Constant	0.038 m^{-1}
c_3	Constant	68 m
c_4	Constant	1 g C (g Chl)$^{-1}$
MLD	Mixed layer depth	m
z	Depth	m
Z_{eu}	Euphotic depth, depth horizon where NPP = 0.01μg C m^{-3} h^{-1}	m

References

Behrenfeld, M. J., Marañón, E., Siegel, D. A. & Hooker, S.B. A photoacclimation and nutrient based model of light-saturated photosynthesis for quantifying oceanic primary production. *Mar. Ecol. Prog. Ser.* **228,** 103-117 (2002).

Behrenfeld, M. J. & Boss, E. The beam attenuation to chlorophyll ratio: an optical index of phytoplankton photoacclimation in the surface ocean? *Deep Sea Research*. **50,** 1537-1549, (2003).

Behrenfeld, M. J., Boss, E., Siegel, D. A. & Shea, D. M. Carbon-based ocean productivity and phytoplankton physiology from space. *Global Biogeochem. Cycles*, **19,** GB1006, doi:10.1029/2004GB002299 (2005).

Behrenfeld, M. J. *et al.* Controls on tropical Pacific ocean productivity revealed through nutrient stress diagnostics. *Nature* **442,** 1025-1028 (2006).

Behrenfeld, M. J., Milligan, A. J. Photophysiological expressions of iron stress in phytoplankton. *Ann. Rev. Mar. Sci.* **5,** 217-246 (2013).

Brzezowki P. *et al.* The gun4 protein plays a regulatory role in tetrapyrrol biosynthesis and chloroplast-to-nucleus signaling in *Chlamydomonas reinhardtii*. *Plant J.* **79,** 285-298 (2014).

Chavez, F. P., Messié, M. & Pennington, J. T. Marine primary production in relation to climate variability and change. *Ann. Rev. Mar. Sci*. **3,** 227-260 (2011).

Chen Y., Durnford, D., Koblizek, M. & Falkowski, P. Plastid regulation of Lhcb1 transcription in the chlorophyte algae *Dunaliella tertiolecta*. *Plant Physiol*. **136,** 3737-3750 (2004).

Cullen, J. J. & Lewis, M. R. The kinetics of algal photoadaptation in the context of vertical mixing. *J. Plankt. Res.* **10,** 1039-1063 (1988).

Durand, M. D., Olson, R. J. & Chisholm, S. W. Phytoplankton population dynamics at the Bermuda Atlantic Time-series Station in the Sargasso Sea. *Deep Sea Res. II* **48,** 1983 – 2003, doi:10.1016/S0967-0645(00)00166-1 (2001).

Durnford, D., Price, J., McKim, S. & Sarchfield, M. Light-harvesting complex gene expression is controlled by both transcriptional and post-transcriptional mechanisms during photoacclimation in *Chlamydomonas reinhardtii*. *Physiol. Plant.* **118,** 193-205 (2003).

Escoubas, J, *et al*. Light intensity regulation of cab gene transcription is signaled by the redox state of the plastoquinone pool. *Proc. Nat. Acad. Sci*. **92,** 10237-10241 (1995).

Falkowski, P. G., Dubinsky, Z. & Wyman, K. Growth-irradiance relationships in phytoplankton1. *Limnol. Oceanogr.* **30,** 311-321 (1985).

Frigerio S. *et al*. Photosynthetic antenna size in higher plants is controlled by the plastoquinone redox state at the post-transcriptional rather than transcriptional level. *J. Biol. Chem.* **282,** 29457-29469 (2007).

Graff, J. R. *et al*. Analytical phytoplankton carbon measurements spanning diverse ecosystems. *Deep Sea Res. I* **102,** 16-25 (2015).

Halsey, K. H. & Jones, B. M. Phytoplankton strategies for photosynthetic energy allocation. *Annu. Rev. Mar. Sci.,* **7,** 265-297 (2015).

Halsey, K. H., Milligan, A. J. & Behrenfeld, M. J. Contrasting strategies of photosynthetic energy utilization drive lifestyle strategies in ecologically important picoeukaryotes. *Metabolites* **4,** 260-280 (2014).

Huot, Y, Babin, M., Bruyant, F., Grob, C., Twardowski, M. S. & Claustre, H. Relationship between photosynthetic parameters and different proxies of phytoplankton biomass in the subtropical ocean. *Biogeosci*. **4,** 853-868. doi:10.5194/bg-4-853-2007 (2007).

Kirk, J. T. O. *Light and Photosynthesis in Aquatic Ecosystems*. Cambridge University Press, Cambridge (1994).

Laws, E. A. & Bannister, T. T. Nutrient- and light-limited growth of *Thalassiosira fluviatilis* in continuous culture, with implications for phytoplankton growth in the ocean. *Limnol. Oceanogr.* **25,** 457–73 (1980).

Lefebvre S. *et al.* Characterization and expression analysis of the Lhcf gene family in *Emiliana huxleyi* (Haptophyta) reveals differential response to light and CO_2. *J. Phycol.* **46,** 123-134 (2010).

Letelier, R. M. *et al.* Temporal variability of phytoplankton community structure based on pigment analysis. *Limnol. Oceanogr.* **38,** 1420-1437 (1993).

Luo T. *et al.* Thioredoxin dedox regulates ATPase activity of magnesium chelatase CHLI subunit and modulates redox-mediated signaling in tetrapyrrole biosynthesis and homeostasis of reactive oxygen species in pea plants. *Plant Physiol.* **159,** 118-130 (2012).

MacIntyre, H. L., Kana, T. M., Anning, T. & Geider, R. J. Photoacclimation of photosynthesis irradiance response curves and photosynthetic pigments in microalgae and cyanobacteria1. *J. Phycol.* **38,** 17-38 (2002).

Maritorena, S., Siegel, D. A. & Peterson, A. R. Optimization of a semianalytical ocean color model for global-scale applications. *Applied Optics* **41,** 2705-2714 (2002).

Mckim, S. & Durnford, D. Translational regulation of light harvesting complex expression during photoacclimation to high light in *Chlamydomonas reinhardtii*. *Plant Physiol. Biochem.* **44,** 857-865 (2006).

Mochizuki N., Brusslan, J., Larkin, R., Nagatani, A. & Chory, J. *Arabidopsis* genomes uncoupled 5 (gun5) mutant reveals the involvement of Mg-chelatase H subunit in plastid-to-nucleus signal transduction. *Proc. Nat. Acad. Sci.*. **98,** 2053-2058 (2000).

Morel, A. *et al.* Examining the consistency of products derived from various ocean color sensors in the open ocean (Case 1) waters in the perspective of a multi-sensor approach. *Remote Sensing Environ*. **111,** 69-88 (2007).

Jassby, A.D. & Platt, T. Mathematical formulation of the relationship between photosynthesis and light for phytoplankton. *Limnol. Oceanogr.* **21,** 540–547 (1976).

Pfannschmidt T., Nilsson, A. & Allen, J. Photosynthetic control of chloroplast gene expression. *Nature*, **397,** 625-628 (1999).

Pfannschmidt, T. & Yang, C. The hidden function of photosynthesis: a sensing system for environmental conditions that regulates plant acclimation responses. *Protoplasma*. **249,** S125-S136 (2012).

Schrader, P. S., Milligan, A. J. & Behrenfeld, M. J. Surplus Photosynthetic Antennae Complexes Underlie Diagnostics of Iron Limitation in a Cyanobacterium. *PLoS ONE* **6,** e18753. doi:10.1371/journal.pone.0018753 (2011).

Silsbe, G. M., Behrenfeld, M. J., Halsey, K. H., Milligan, A. J. & Westberry, T. K. An accurate absorption-based net primary production model of the global ocean. *In prep for: Global Biogeochem. Cycl.* (2015).

Smith, R. E. H. & Geider, R.J. Kinetics of intracellular carbon allocation in a marine diatom. *J. Exp.Mar. Biol. Ecol.* **93,** 191–210 (1985).

Stenbaek, A. & Jensen P. E. Redox regulation of chlorophyll biosynthesis. *Phytochemistry* **71,** 853–859 (2010).

Sunda, W. G. & Huntsman, S. A. Iron uptake and growth limitation in oceanic and coastal phytoplankton. *Mar. Chem*. **50,** 189-206 (1995)

Tang, E., Vincent, W. Effects of daylength and temperature on the growth and photosynthesis of an Arctic cyanobacterium, *Schizothrix calcicola* (Oscillatoriaceae). *Eur. J. Phycol*. **35,** 263-272 doi: 10.1080/09670260010001735861 (2000).

Vandenabeele, S. *et al*. Catalase deficiency drastically affects gene expression induced by high light in *Arabidopsis thaliana*. *Plant J*. **39,** 45– 58 (2004).

Verity, P. G. Effects of temperature, irradiance, and daylength on the marine diatom *Leptocylindrus danicus* Cleve. I. Photosynthesis and cellular composition. *J. Exper. Mar. Biol. Ecol.* **55,** 79-91 (1981).

Westberry, T. K., Behrenfeld, M. J., Siegel, D. A. & Boss, E. Carbon-based primary productivity modeling with vertically resolved photoacclimation. *Global Biogeochem. Cycles*. **22,** GB2024, doi:10.1029/2007GB003078 (2008).

Winn, C. D. *et al*. Seasonal variability in the phytoplankton community of the North Pacific Subtropical Gyre. *Global Biogeochem. Cycl.* **9,** 605-620 (1995).

Wobbe L., Schwarz, C.,Nickelsen, J. & Kruse, O. Translational control of photosynthetic gene expression in phototrophic eukaryotes. *Physiologia Plantarum*. **133,** 507-515 (2008).